Journal of Solid State Chemistry **148,** 205–214 (1999)
Article ID jssc.1999.8433, available online at http://www.idealibrary.com on IDEAL®

Structure and Crystal Chemistry as a Function of Composition across the Wide Range Nonstoichiometric $(1-\varepsilon)ZrO_2 \cdot \varepsilon SmO_{1.5}$, $0.38 < \varepsilon < 0.55$, Oxide Pyrochlore System

Yasunori Tabira[1] and Ray L. Withers

Research School of Chemistry, Australian National University, Canberra, A.C.T., 0200, Australia

Received March 24, 1999; in revised form June 9, 1999; accepted June 29, 1999

The extent of the pyrochlore solid solution field (at 1500°C) in the $(1-\varepsilon)ZrO_2 \cdot \varepsilon SmO_{1.5}$ system has been determined as running from 38.5 to 55 mol% $SmO_{1.5}$. Subtle changes in crystal structure have been investigated as a function of composition across this solid solution field using a wide-angle convergent beam electron diffraction technique. Systematic changes in the one unknown oxygen atom fractional coordinate x are found as a function of composition and investigated from a crystal chemical point of view using the bond length – bond valence approach. The parameter x is found to be ~ 0.352 for $\varepsilon = 0.40$ and 0.348 for $\varepsilon = 0.45$ and 0.55. Both values of x are significantly larger than the value ($x = 0.342$) found for the stoichiometric 50 mol% $SmO_{1.5}$ specimen by the same technique. The increased x value found for nonstoichiometric compositions on either side of the ideal pyrochlore composition ($\varepsilon = 0.5$) is consistent with a systematic shift toward the average value for this parameter in the so-called "defect fluorite" structure ($x = 0.375$), the phase field for which appears on either side of the relevant pyrochlore solid solution field.

1. INTRODUCTION

Rare earth oxide pyrochlores, ideal stoichiometry $(Ln^{3+})_2(M^{4+})_2(O1)_6(O2)_1$ (Ln a lanthanide), can be described as $2 \times 2 \times 2$ fluorite-related superstructure phases and crystallize in space group $Fd3m$ (origin choice 2) with four crystallographically independent atom sites (Ln in 16d at 1/2, 1/2, 1/2, M in 16c at 000, O1 in 48f at x, 1/8, 1/8, and O2 in 8b at 3/8, 3/8, 3/8) (see Fig. 1) (1). The metal ions form an ordered, ccp eutactic cation array with O1 ions occupying off-center sites within Ln_2M_2 tetrahedra and O2 ions Ln_4 tetrahedral sites therein. There is only one free positional parameter, the x fractional coordinate of O1. For a regular octahedral oxygen environment around M, x should be 0.3125 whereas, for a regular cubic oxygen environment around A (as in the unmodulated fluorite type parent structure), x should equal 0.375. The deviation of x from 0.375 is thus a sensitive measure of the difference between a pyrochlore and a "defect fluorite" phase (1, 2).

Significant ranges of stoichiometry on either side of the ideal $Ln_2M_2O_7$ composition as well as order–disorder transformations at high temperature from pyrochlore to disordered defect fluorite are known to occur in the case where M = Zr (3–8). Such rare earth zirconate pyrochlore solid solutions occur in $(1-\varepsilon)ZrO_2 \cdot \varepsilon LnO_{1.5}$ systems for the lighter rare earth elements (Ln = La–Gd) around the composition $\varepsilon \sim 0.5$. For the heavier rare earth elements beyond Gd, only a disordered defect fluorite phase is found. In those cases where a pyrochlore phase does occur, there is usually a high temperature order–disorder phase transition from pyrochlore to the defect fluorite phase before melting (5). This transition temperature is lowest for Ln = Gd ($\sim$1530°C) and increases systematically as the size of the dopant rare earth ion increases until Ln = La where the phase transition no longer takes place and the pyrochlore phase is stable all the way up to the melting point.

Conventional wisdom suggests that the region of stability of the pyrochlore solid solution field necessarily shrinks with respect to both composition and temperature in going from Ln = La to Ln = Gd (1–11). Recently, however, a careful synthesis and XRPD study has shown that the composition width of the pyrochlore solid solution field in the $(1-\varepsilon)ZrO_2 \cdot \varepsilon LaO_{1.5}$ system (for specimens rapidly quenched from 1500°C) is considerably narrower than previously reported (certainly less than 2 mol% $LaO_{1.5}$ in width). From a crystal chemical point of view, one might expect that the composition width of a pyrochlore solid solution would be largest when the cation size difference is smallest. Such a consideration would suggest the largest composition width for Ln = Gd with a continuously narrowing solid solution width as the rare earth ion heads toward La. Unfortunately the proximity of the high temperature pyrochlore to defect fluorite phase transition (at 1530°C) to the necessary temperatures of synthesis in order to approach equilibrium in a reasonable time frame (a few weeks) means that the Ln = Gd system is not the ideal

[1]To whom all correspondence should be addressed.

0022-4596/99 $30.00

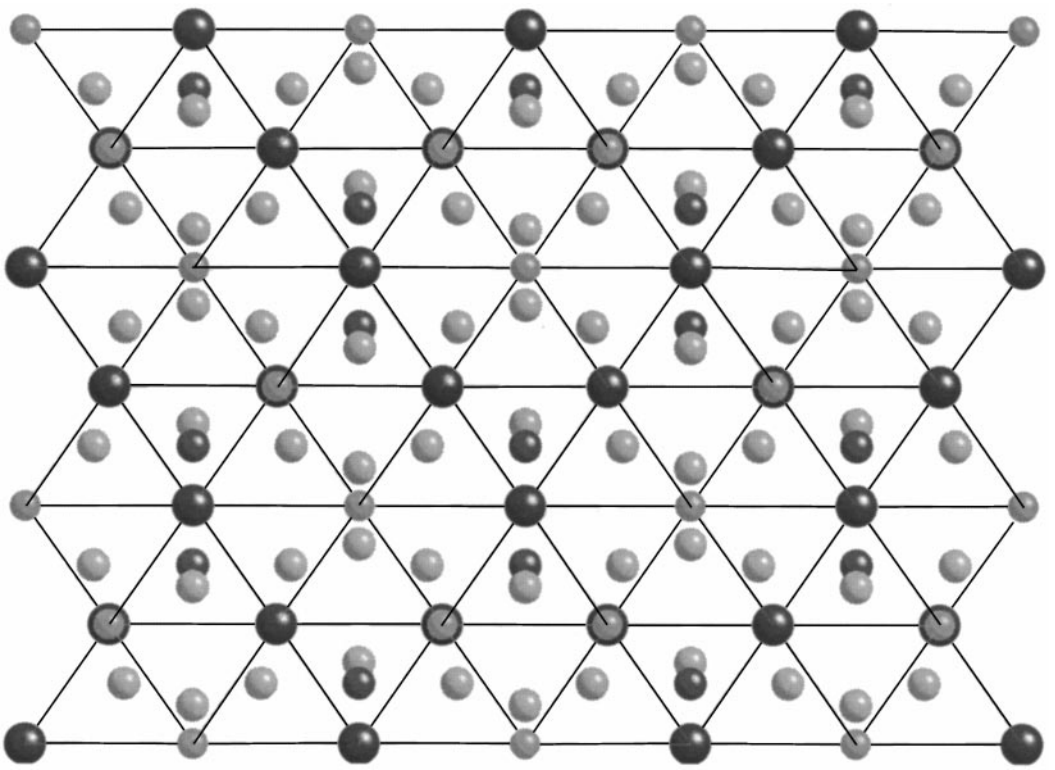

FIG. 1. The ideal pyrochlore structure type shown in projection along ⟨110⟩. Lines are shown connecting nearest neighbor metal ions forming the ccp cation array (light, *M*; dark, *Ln*). O1 ions (light) are off-center positions in Ln_2M_2 tetrahedra whereas O2 ions (dark) are at the center of Ln_4 tetrahedra.

system to test this hypothesis. (The extremely slow kinetics for cation ordering in such systems necessitates a relatively high temperature of synthesis, $> \sim 1400^\circ$C). In the case of the $Ln = $ Sm system, however, the pyrochlore to defect fluorite phase transition takes place at a sufficiently high temperature ($\sim 2000^\circ$C) that a determination of the pyrochlore solid solution width is feasible at a temperature ($\sim 1500^\circ$C) at which the kinetics of cation ordering do not prevent equilibrium from being attained. The determination of the pyrochlore solid solution width in the $Ln = $ Sm system at 1500°C is one aim of the current paper.

Given that oxygen ion conductivity is strongly dependent upon composition in such systems (9–11) a related aim is to use a recently developed quantitative wide-angle convergent beam electron diffraction (WACBED) technique to investigate systematic structural changes in the one unknown oxygen atom fractional coordinate x as well as in the thermal parameters of the constituent ions as a function of composition across the solid solution field. (This technique has recently been successfully applied to extract unknown oxygen atom fractional coordinates from two separate oxide systems (12, 13).) Such studies are essential in order to obtain insight into the crystal chemistry and ionic conductivity properties of rare earth zirconate pyrochlores (see, for example, (9, 10)). To date, there has been only one reported experimentally determined x value for a rare earth zirconate pyrochlore (that for stoichiometric $La_2Zr_2O_7$ (14)) and none at all for an off-stoichiometric pyrochlore.

2. EXPERIMENTAL

Synthesis

Samples were prepared from the starting materials Sm_2O_3 (Research Organic/Inorganic Chemical Corp. 99.9%) and ZrO_2 (Z-Tech > 99.9%, including 2.57% HfO_2) by grinding in the appropriate ratio, pelleting, and calcining. The initial starting materials were first fired at 1000°C for a day before weighing. Sm_2O_3 was found to be extremely hygroscopic. On standing in the laboratory under atmospheric conditions for more than an hour or two, the reagent grade Sm_2O_3 was found via XRPD to transform from the nominal B-type sesquioxide into $Sm(OH)_3$ (S.G. = $P6_3/m$, $a_0 = 6.371(1)$ Å, $c = 3.680(1)$ Å). The desired B-type sesquioxide Sm_2O_3 starting material (S.G. = $C2/m$, $a = 14.177(5)$ Å, $b = 3.6295(8)$ Å, $c = 8.8506(5)$ Å and $\beta = 100.01(5)^\circ$) was obtained after the 1000°C heat treatment.

Compositions ranging from 30 mol% $SmO_{1.5}$ through stoichiometric $Sm_2Zr_2O_7$ up to 60 mol% $SmO_{1.5}$ were thoroughly mixed mechanically before being pressed into

pellets, placed in stabilized zirconia crucibles, and heated at 1500°C for three days followed by repelleting before heating again at 1500°C for a further three days. In order to achieve equilibrium, it was subsequently found necessary to regrind, repellet, and reheat for a further 7 days. Platinum supports and vessels were avoided due to the reaction of platinum with the lighter rare earth element containing specimens. The pellets were subsequently quenched in water from 1500°C. XRD patterns using a Guinier–Hägg camera with monochromated Cu$K\alpha_1$ radiation (25 mA × 40 kV) were taken to calculate the cell constants and to determine the extent of the pyrochlore solid solution field.

Wide-Angle Convergent Beam Electron Diffraction

Specimens for electron microscope investigation were prepared by crushing and dispersing onto holey-carbon coated copper grids. WACBED patterns of these crushed polycrystalline specimens were taken using a Philips EM430 electron microscope, operating at 300 kV. The area irradiated on a crystal fragment was typically around 50 nm. 111* systematic row geometry was used. Typically the 11, 11, 11 reflection was tilted close to the exact Bragg condition in selected area diffraction mode and the incident beam then converged to give rise to a WACBED pattern. The convergence angle of the incident beam around $\theta_{11,11,11}$ (typically $\sim 0.4^\circ$) corresponds to reflections from $g = 777$ to 15, 15, 15 being excited in the 11, 11, 11 CBED disk (see Fig. 2). The diffraction geometry and experimental conditions employed have been described in more detail elsewhere and hence will not be repeated here (12).

Relevant WACBED patterns recorded on unsaturated film negatives were digitized by a scanner into 8-bit image depth using 300–600 dpi resolution, which typically yielded about 300 data points in a line profile. Areas suffering from nonsystematic K-line crossings were avoided as much as possible. A line profile perpendicular to the experimentally observed diffraction lines within the 11, 11, 11 CBED disk was obtained after averaging the intensity pixel by pixel along the diffraction lines. Then the pixel units were transformed into k_x, the projection component of the incident beam wavevector k_0 on to the zero order Laue zone (ZOLZ) plane in units of the length of the relevant reciprocal lattice vector—in this case $|g_{111}|$. Subsequently a polynomial function was used to subtract background.

The specimen thickness was estimated from the diffraction line widths via a comparison with calculated WACBED line profiles. Typical average thicknesses were usually in the

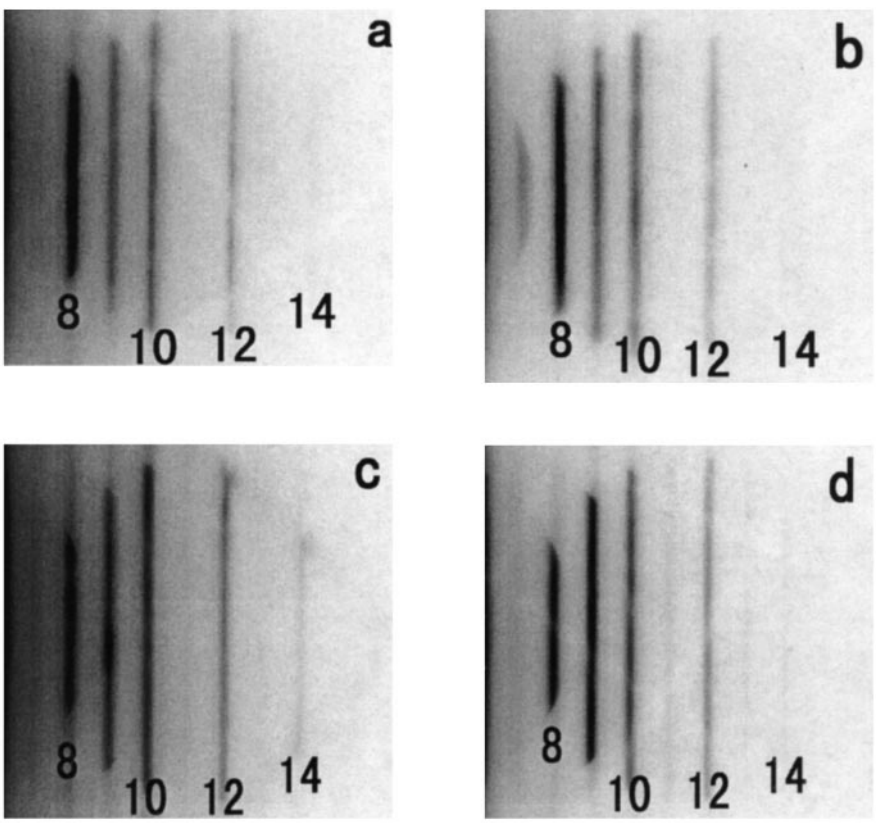

FIG. 2. Experimental WACBED patterns as a function of stoichiometry in the $(1-\varepsilon)ZrO_2 \cdot \varepsilon SmO_{1.5}$ system. (a) $\varepsilon = 0.4$, (b) $\varepsilon = 0.45$, (c) $\varepsilon = 0.5$, and (d) $\varepsilon = 0.55$. The numbers indicate the order of the *hhh* reflections.

100–180 nm range. A fully dynamical calculation utilizing the appropriate electron scattering factors (15) was carried out as a function of the inclination of the incident beam over orientations ranging from $k_x/g_{111} = 3.75$ up to $k_x/g_{111} = 7.25$ at intervals of 0.0125, including 35 beams from -8, -8, -8 up to 26, 26, 26 on the 111* systematic reciprocal-space row. The thickness variation which inevitably exists to some extent in any illuminated area of crushed powder was taken into account by averaging the simulated line profiles for five different thicknesses up to $\pm 10\%$ around the average thickness (12). To ensure that dynamical diffraction effects were adequately taken into account, it was required that the structural parameters obtained fitted experimentally obtained WACBED line profiles at several different average thicknesses.

3. RESULTS

Powder XRD Results

The extent of the pyrochlore solid solution in the $(1-\varepsilon)ZrO_2 \cdot \varepsilon SmO_{1.5}$ system is rather poorly defined. Two phase regions, for example, have never been shown between the pyrochlore and defect fluorite phase fields (2–5). Partially this is because it is difficult to distinguish between pyrochlore and defect fluorite (8)—pyrochlore is after all a fluorite-related superstructure phase (see, for example, the $\langle 110 \rangle$ zone axis electron diffraction patterns of the (a) 35, (b) 50, and (c) ~ 60 mol% $SmO_{1.5}$ specimens shown in Fig. 3. Note that (a) and (c) are in the defect fluorite phase field whereas (b) is in the pyrochlore phase field). Collongues *et al.* (4) reports a composition range of existence from 37.4 to 60.1 mol% $SmO_{1.5}$ at 1450°C. A rather similar composition range of existence is reported in Perez y Jorba (3) and Bevan and Summerville (8), although again two phase regions between pyrochlore and defect fluorite phase fields were not reported. In order to more accurately determine the width and composition range of the pyrochlore solid solution field (at 1500°C), samples were prepared at compositions ranging from 30 to 60 mol % $SmO_{1.5}$ in 2.5 mol% steps as described above and then quenched from 1500°C.

Figure 4 shows the resultant refined lattice parameter data for the specimens heated for 6 days (open symbols) and 13 days (filled symbols). Triangles and squares indicate the pyrochlore and defect-fluorite phase, respectively, the latter being plotted as $2a_0$ for convenience. Equilibrium was adjudged to have been achieved when further subsequent heating led to no further significant change. It can be seen that heating for 13 days was certainly necessary on the low $SmO_{1.5}$ content side. The onset of a two phase region separating the pyrochlore and defect fluorite phase fields was easily detected at 55 mol% $SmO_{1.5}$ on the high $SmO_{1.5}$ side of the pyrochlore field. On the low $SmO_{1.5}$ side, however, no two-phase region was ever directly detected. The existence of a narrow two phase region (<2.5 mol% in width) was inferred from the refined lattice parameter data for the 13 days heated specimens shown in Fig. 4. It can be seen that the extent of the pyrochlore solid solution field

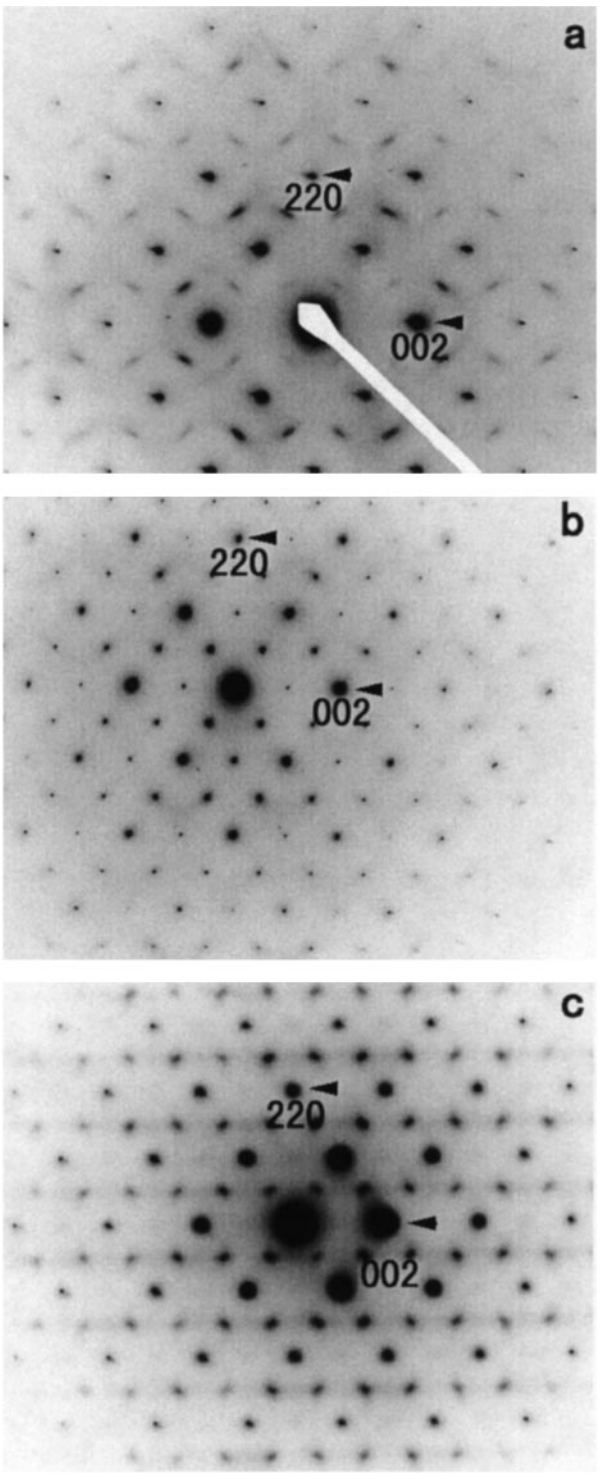

FIG. 3. Typical $\langle 110 \rangle$ zone axis electron diffraction patterns of (a) $\varepsilon = 0.35$, (b) $\varepsilon = 0.50$, and (c) $\varepsilon = 0.60$ specimens. Both (a) and (c) are in the defect-fluorite phase field whereas (b) is characteristic of a specimen within the pyrochlore phase field.

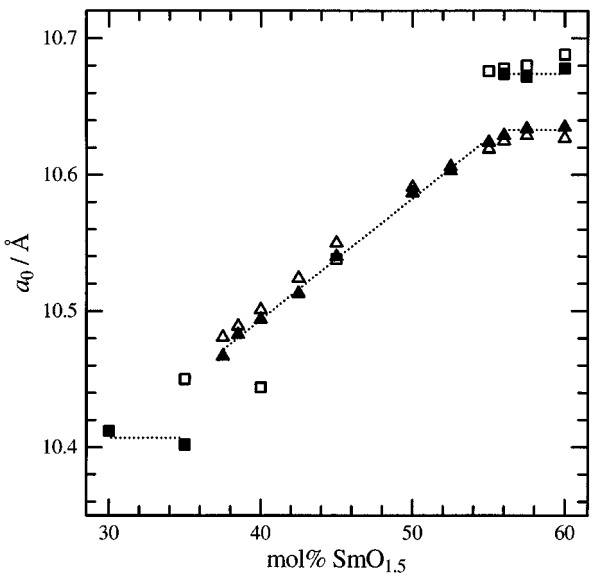

FIG. 4. Variation of the pyrochlore cell constant as a function of stoichiometry. The open symbols are for specimens annealed for 6 days at 1500°C and the closed symbols are for 13 day annealed specimens at the same temperature. Triangles, pyrochlore; squares, defect fluorite. $2a_0$ is plotted for defect fluorite.

ranges from ~38.5 to 55 mol% $SmO_{1.5}$. The end member pyrochlore unit cell dimension on the lower $SmO_{1.5}$ side was found to be 10.467(1) Å while that on the higher $SmO_{1.5}$ side was 10.635(1) Å. The significant difference (~0.17 Å) between these end member pyrochlore unit cell dimensions is consistent with a rather broad solid solution in the Ln = Sm case. In the $(1-\varepsilon)ZrO_2 \cdot \varepsilon LaO_{1.5}$ system, by contrast, the difference in end member lattice parameters is only ~0.016 Å. It is clear that the width of the pyrochlore solid solution does indeed increase, rather than decrease, in going from Ln = La to Gd.

Structural Models for Nonstoichiometric $(1-\varepsilon)ZrO_2 \cdot \varepsilon SmO_{1.5}$ (ε = 0.4, 0.45, 0.50 and 0.55) Pyrochlores by Quantitative WACBED

Figure 2 shows experimentally obtained WACBED patterns (obtained at a similar average thickness) for ε = (a) 0.40, (b) 0.45, (c) 0.50, and (d) 0.55 across the pyrochlore solid solution field. Note the systematic changes observed in the experimental WACBED patterns as a function of composition. Thus, for example, the 888 reflection systematically increases in intensity relative to the 999 and 10, 10, 10 reflections as ε is reduced from the stoichiometric composition of $\varepsilon = 0.5$ toward the low Sm content end of the solid solution. Similarly, there is a systematic increase in the intensity of the 999 reflection relative to the 888 and 10, 10, 10 reflections as ε is increased from the stoichiometric composition of $\varepsilon = 0.5$ toward the high Sm content end of the solid solution. Note that because the excited reflections occur a long way out in reciprocal space, WACBED patterns are typically rather more sensitive to changes in displacive parameters (such as fractional coordinates or thermal parameters) than they are to changes in compositional parameters (such as site occupancies).

For this reason, the resultant WACBED line profiles are relatively insensitive to the exact occupancies of the available crystallographic sites of the space group $Fd\bar{3}m$ of the pyrochlore structure type. In order to propose a reasonable model for the observed systematic changes as a function of stoichiometry, it is therefore worthwhile to begin by making a comparison of simulated line profiles as a function of displacive parameters assuming occupancies appropriate only for the stoichiometric composition $Sm_2Zr_2O_7$ (instead of for real nonstoichiometric compositions such as, e.g., $Sm_{1.6}Zr_{2.4}O_{7.2}$ for $\varepsilon = 0.4$ etc.).

Figure 5 shows calculated WACBED line profiles (at a thickness of 140 nm) for stoichiometric $Sm_2Zr_2O_7$ as a function of the one unknown oxygen atom fractional coordinate (the x parameter of the O1 atom) ranging from $x = 0.342$ (12) up to $x = 0.375$ (the value that would be appropriate for the defect fluorite phase). As x increases from 0.342, it is clear that I_{888} systematically comes up relative to the other excited reflections in a qualitatively rather similar manner to that observed in the experimental WACBED patterns as ε reduces from 0.5 toward 0.4 (see Figs. 2a–2c). The clear implication is that samarium poor compositions relative to the ideal pyrochlore stoichiometry are characterized by increased values of x.

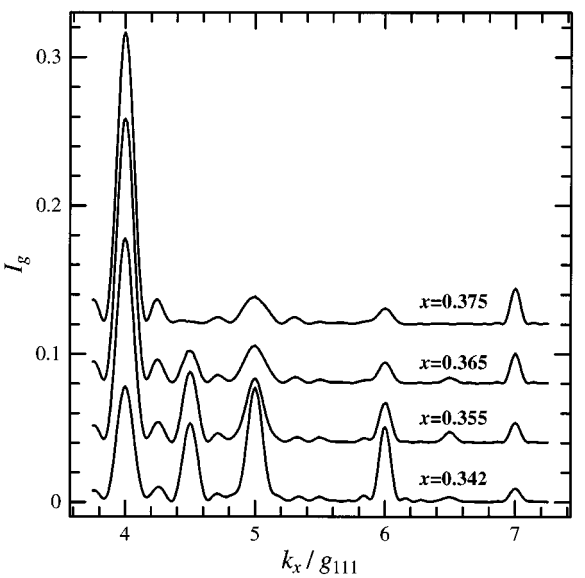

FIG. 5. Systematic change in calculated WACBED line profiles as a function of the unknown fractional coordinate x of the O1 oxygen atom for stoichiometric $Sm_2Zr_2O_7$ at a thickness of 140 nm. The inclination of the incident beam is defined by the projected component of its wavevector k_0 onto the 111* reciprocal axis k_x in units of the length of 111 reciprocal lattice vector g_{111}.

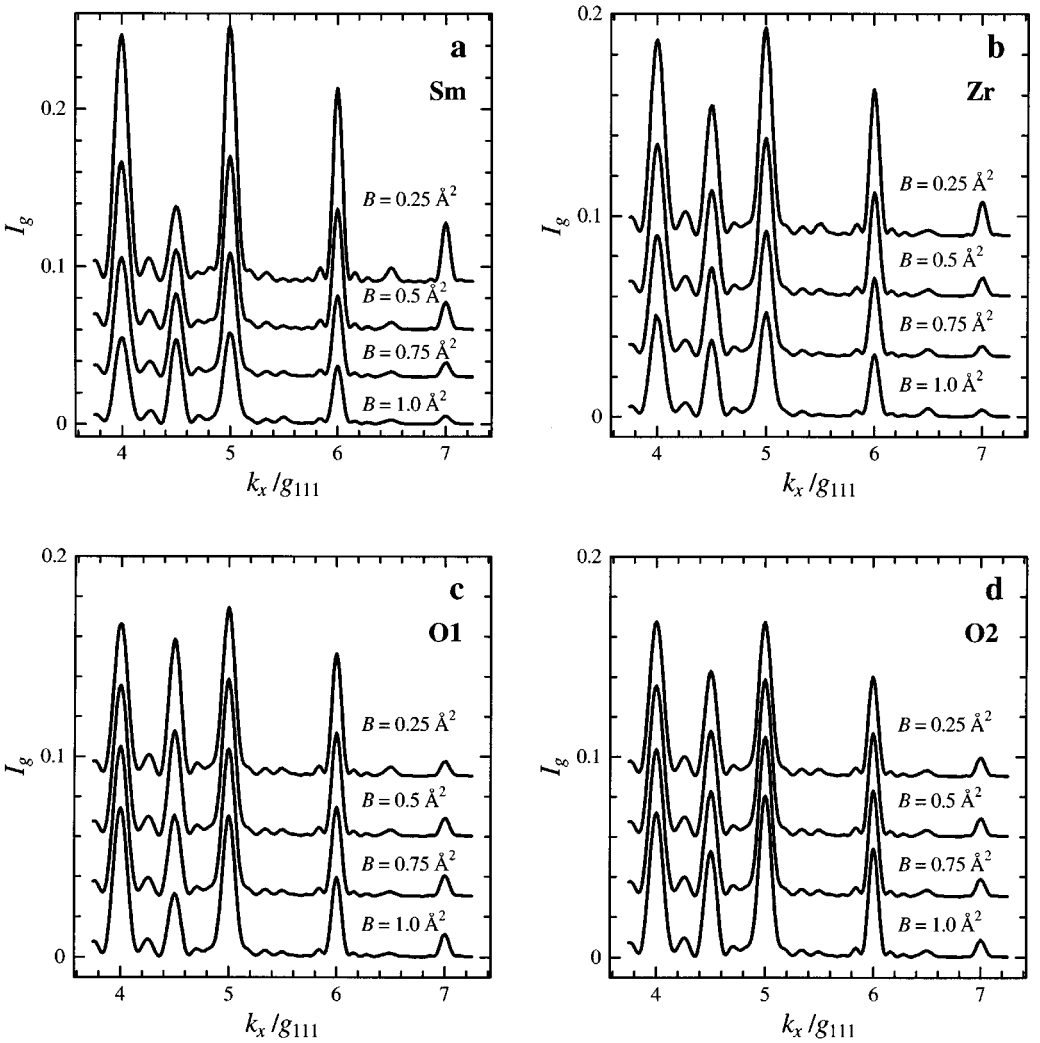

FIG. 6. The change of WACBED line profiles for four different kinds of isotropic temperature factor B's on each site ranging from 0.25 to 1.0 Å^2 for stoichiometric $Sm_2Zr_2O_7$. The nonvarying B factors in each plot are 0.5 Å^2 and the thickness is 140 nm.

In the case of the high $SmO_{1.5}$ line profile, however, I_{999} is clearly stronger than I_{888} and $I_{10,10,10}$. Such an effect cannot be achieved by altering x alone. It is qualitatively clear that another displacive structural parameter, an isotropic thermal parameter, must be significantly altered from its value for stoichiometric pyrochlore in order to achieve a satisfactory fit to the experimentally observed WACBED line profile. Figure 6 shows how calculated WACBED line profiles for stoichiometric $Sm_2Zr_2O_7$ change as a function of the isotropic temperature factors (B's of the form $\exp(-B\sin^2\theta/\lambda^2)$) on the *Ln*, Zr, O1, and O2 crystallographic sites. Thicknesses were assumed to be 140 nm for this calculation (no thickness averaging applied). Owing to its small content as well as relatively low scattering power, altering B_{O2} has very little effect on the calculated WACBED line profile (see Fig. 6d). The effect of altering B_{Zr} is likewise not dramatic, leading mainly to a change in the overall scale of the calculated line profile (see Fig. 6b). (As a result, B_{Zr} and B_{O2} were both fixed to be 0.5 Å^2 in all of the calculations hereafter). On the other hand, increasing B_{Sm} significantly reduces the intensity, I_{hhh} (h, even), of the even order reflections while altering the calculated intensity of the 999 reflection, I_{999}, only marginally (see Fig. 6a). Increasing B_{O1} affects the relative intensities of the various excited reflections in a slightly more complicated manner—the intensities of the 999 and 12, 12, 12 reflections, I_{999} and $I_{12,12,12}$, diminish relative to the intensities of the 888 and 10, 10, 10 reflections, I_{888} and $I_{10,10,10}$, as B_{O1} increases (see Fig. 6c).

Having considered the first order effect of the available displacive structural parameters it is clear that obtaining a fit to the high $SmO_{1.5}$ line profile will require increasing

B_{Sm} and/or decreasing B_{O2} relative to those obtaining for the stoichiometric composition.

The experimentally determined extent of the pyrochlore single phase region, from $\sim$38.5 up to 55 mol% $SmO_{1.5}$, requires that the *Ln* (16*d* in Wyckoff notation) site (for the samarium poor side) and the Zr site (16*c*) (for the samarium rich side) are occupied by both Sm and Zr. From a crystal chemical point of view, it is interesting to note that both these situations imply an increase of the unknown oxygen atom *x* value—on the samarium poor side, in order to decrease the *Ln*–O1 bond distance so that the 16*d* site can be suitable for accommodation by smaller Zr ions and, on the samarium rich side, in order to increase the Zr–O1 distances so that the 16*c* site can be suitable for larger *Ln* ions.

For the purposes of calculation, we fixed the cation distribution over the metal ion 16*d* and 16*c* sites as $\text{occ}(16d) = 2\varepsilon\text{Sm} + (1-2\varepsilon)\text{Zr}$, $\text{occ}(16c) = \text{Zr}$ for $x \le 0.5$ and $\text{occ}(16d) = \text{Sm}$, $\text{occ}(16c) = (2-2\varepsilon)\text{Zr} + (2\varepsilon-1)\text{Sm}$ for $x > 0.5$ (see Table 1). This need not necessarily be true. It is, however, one of the simplest possible cation ordering models and any deviation would only have a relatively minor effect on the calculated WACBED patterns for the reason described above. The extra $(1-2\varepsilon)$ oxygens per formulae unit required from charge balance considerations for $\varepsilon < 0.5$ were introduced as O3 atoms (on 8*a* sites) and it was assumed that the O1 and O2 sites were fully occupied, corresponding to the choice $G_{O3} = (1-2\varepsilon)$ in Table 1. The unknown fractional coordinate *x* of O1 was then determined to be $\sim$0.352 for $\varepsilon = 0.4$, associated with isotropic temperature factors B_{Sm} and B_{O1} given by 0.75 and 1.0 Å^2, respectively. The excellent resultant fit is depicted in Fig. 7a. One difficulty of this average structure model is that, despite the significant increase in *x* toward the value appropriate for a defect fluorite, it still produces rather short O3–O2 distances of 2.38 Å. In the case of the 45 mol% specimen, a good fit to the observed WACBED line profile was obtained for $x = 0.348$ with $B_{Sm} = B_{O1} = 1.0$ Å^2 (see Fig. 7b).

TABLE 1
$(1-\varepsilon)\text{ZrO}_2 \cdot \varepsilon\text{SmO}_{1.5} \equiv \text{Sm}_{4\varepsilon}\,\text{Zr}_{4-4\varepsilon}\text{O}_{8-2\varepsilon}$

Sites	Occupancies	Coordinates
	$\varepsilon \le 0.5$	
16*d*	$2\varepsilon\text{Sm} + (1-2\varepsilon)\text{Zr}$	1/2, 1/2, 1/2
16*c*	Zr	0, 0, 0
48*f*	1	*x*, 1/8, 1/8
8*b*	$(2-2\varepsilon) - G_{O3}$	3/8, 3/8, 3/8
8*a*	G_{O3}	1/8, 1/8, 1/8
	$\varepsilon \ge 0.5$	
16*d*	Sm	1/2, 1/2, 1/2
16*c*	$(2-2\varepsilon)\text{Zr} + (2\varepsilon-1)\text{Sm}$	0, 0, 0
48*f*	1	*x*, 1/8, 1/8
8*b*	$(2-2\varepsilon) - G_{O3}$	3/8, 3/8, 3/8
8*a*	G_{O3}	1/8, 1/8, 1/8

In the case of the 55 mol% $SmO_{1.5}$ specimen, a good fit to the experimentally observed line profile was obtained for $x \sim 0.348$, B_{Sm} (=1.5 Å^2) and B_{O1} (=0.75 Å^2). The resultant fit is shown in Fig. 7d. The relatively large B_{Sm} (=1.5 Å^2) required to obtain a good fit to the experimentally observed data can be rationalized in terms of O2 oxygen vacancies required on the high $SmO_{1.5}$ of the solid solution field (see Table 1). Such oxygen ions are strongly bonded to four neighboring 16*d* atoms in the form of an (O2) $(Ln)_4$ tetrahedron. Vacancies on this site could be expected to have a significant effect on the temperature factor of the 16*d* site cations, particularly along $\langle 111 \rangle$ directions.

WACBED line profiles were experimentally typically quite robust (see, for example, the $\varepsilon = 0.4$ WACBED patterns taken at the quite different average thicknesses of 100 and 160 nm, shown in Figs. 8a and 8b). It is nonetheless important that the structural models derived above should fit experimental WACBED data at more than one average thickness. This was the case for all compositions examined. That it was so for the 40 mol% $SmO_{1.5}$ specimen is shown in Fig. 8.

4. DISCUSSION

While one cannot directly determine exact local configurations from the average structure of a nonstoichiometric pyrochlore determined by WACBED, it is nonetheless possible to infer useful local structural information via the bond length–bond valence approach (16–18). Consider, for example, how the pyrochlore structure type might accommodate reducing $SmO_{1.5}$ content away from the ideal stoichiometric composition. Reducing $SmO_{1.5}$ content necessitates replacing a certain proportion of the Sm ions on the 16*d* sites with Zr ions (20%, for example, in the case of the 40 mol% $SmO_{1.5}$ pyrochlore—see Table 1) and the simulataneous incorporation of extra oxygen atoms (nominally 0.2 per formula unit for the 40 mol% $SmO_{1.5}$ pyrochlore) onto the O3 or 8*a* (1/8, 1/8, 1/8) sites. Zr's on the 16*d* sites will, of necessity, be heavily underbonded (AV $\sim$ 2 instead of the ideal 4). The extra oxygens on the O3 sites are not, however, bonded to these ions but rather to the Zr ions on the 16*c* sites. This causes two coupled crystal chemical problems. First, one cannot use the extra O3 oxygen ions to improve the underbonding of the Zr's on the 16*d* sites. The only way to improve the apparent valence (V_i) of these Zr ions is to increase *x* or to shrink the cell parameter or both. Second, the presence of O3 ions causes the initially happily bonded Zr's on the 16*c* sites to become overbonded. This could be overcome by a combination of increasing *x* and requiring that only one of the two O3 sites bonded to a 16*c* Zr be occupied.

Increasing *x* by $\sim$0.1, from 0.342 for the ideal stoichiometric composition to 0.352 as determined experimentally for the 40 mol% $SmO_{1.5}$ pyrochlore (see Fig. 9) improves

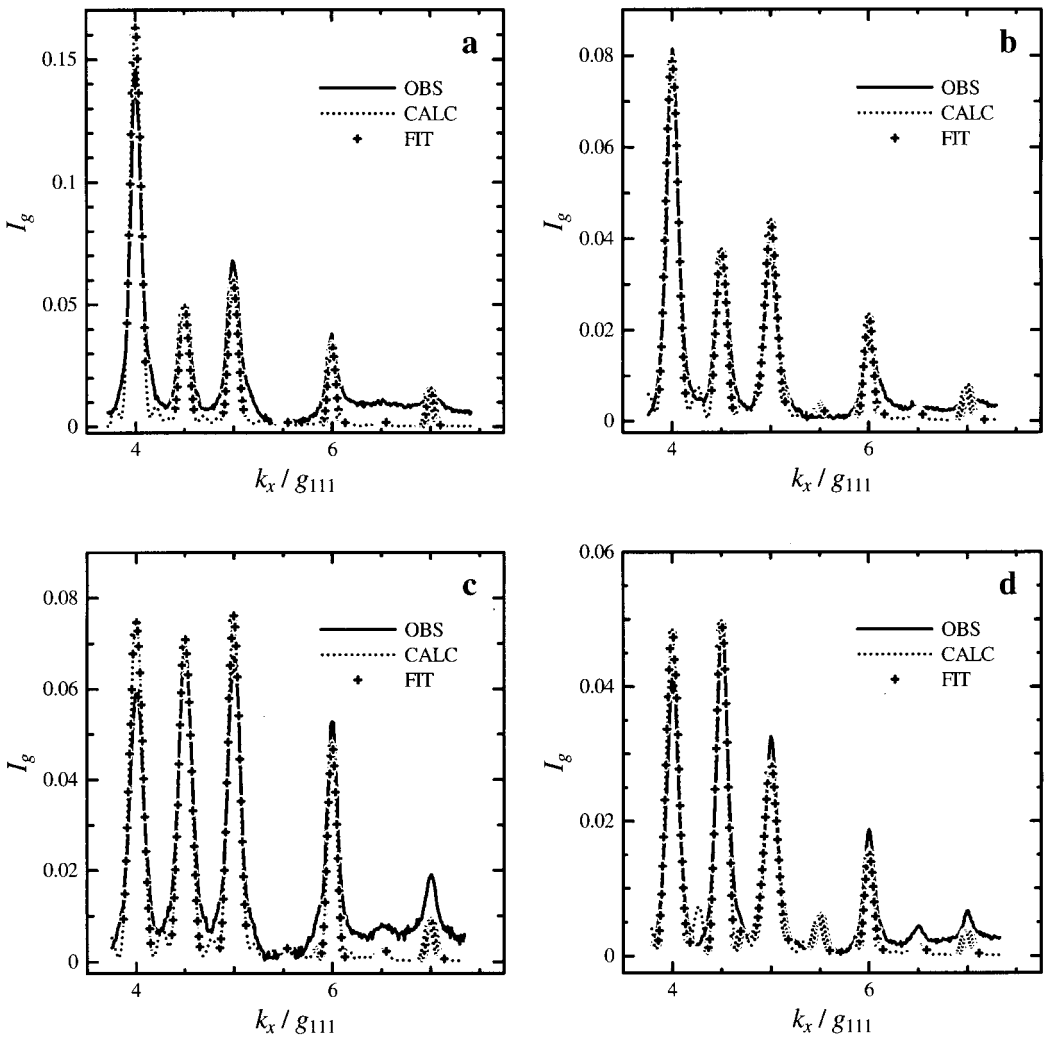

FIG. 7. Shows the best fit to the observed WACBED line profiles for the (a) 40, (b) 45, (c) 50, and (d) 55 mol% $SmO_{1.5}$ specimens. The unknown fractional coordinate x of the O1 oxygen atom was found to be 0.352, 0.348, 0.342, and 0.348, respectively, with associated isotropic temperature factors as given in the text.

the underbonding of the Zr ions on the 16*d* sites. At the same time, however, it will make the originally happily bonded Sm ions on this site significantly overbonded if both O2 sites bonded to such a Sm ion are occupied (see curve *c* in Fig. 9). If only one such O2 site is occupied, however, then the Sm ion will be happily bonded (see curve b in Fig. 9). Likewise, increasing x to 0.352 makes the originally happily bonded Zr ions on the 16*c* site underbonded sufficiently (see curve d in Fig. 9) that one of the O3 sites bonded to such a Zr ion can probably now be occupied (see curve e in Fig. 9). In Fig. 9, the calculated valence for a Sm on a 16*d* site with zero, one, and both neighboring O2 sites occupied is plotted as function of x. The calculated valence for a Zr on a 16*c* site is also plotted as a function of x for zero, one, and both neighboring O3 sites occupied. It can clearly be seen that the Sm's on the 16*d* site would be most comfortable with only one neighboring O2 site whereas the Zr's on the 16*c* site need at least one neighboring O3 site to be occupied for the experimentally observed value for x of 0.352 at $\varepsilon = 0.4$. The Zr's on the 16*d* site are least underbonded when both of the neighboring O2 sites are occupied. For the 40 mol% $SmO_{1.5}$ structural model, the most likely average occupancies on the three available oxygen sites are therefore 1 for the O1 site, 0.6 for the O2 site, and 0.6 again for the O3 site, rather than 1, 1, and 0.2, respectively. (Note that the changed occupancies on the O2 and O3 sites do not affect the quality of the fit to the WACBED data in Fig. 7.) Such considerations suggest the existence of strong local ordering rules which might be expected to give rise to short range order and possibly structured diffuse scattering. It is noted that a characteristic but very weak diffuse distribution was observed in the nonstoichiometric specimens.

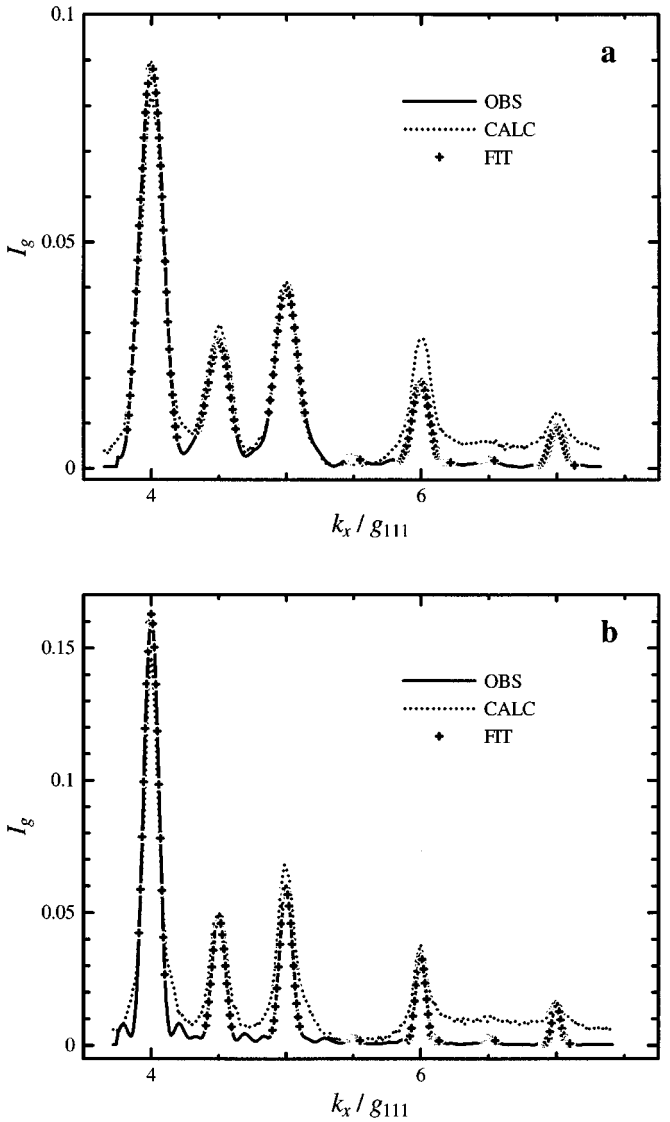

FIG. 8. Shows fitted WACBED line profiles of the 40 mol% $SmO_{1.5}$ specimen at two quite different average thicknesses: (a) 100 and (b) 160 nm. In both cases, the same structural model was used, i.e., $x = 0.352$ with associated isotropic temperature factors $B_{Ln} = 0.75$ Å^2, $B_{Zr} = 0.5$ Å^2, $B_{O1} = 1$ Å^2, and $B_{O2} = 0.5$ Å^2.

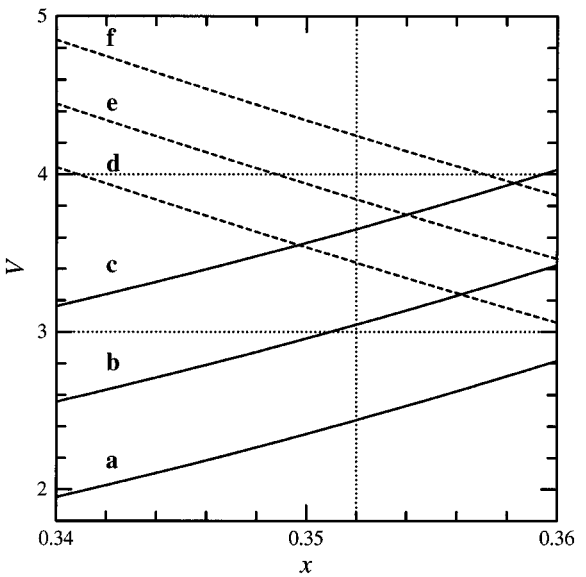

FIG. 9. Calculated bond valences, V_i, for a Sm ion on the 16*d* site and a Zr ion on the 16*c* site as a function of the one unknown fractional coordinate, x, of the O1 oxygen ion. The calculation assumes (a) zero, (b) one, and (c) two O2 ions are bonded to the Sm ion and (d) zero, (e) one, and (f) two O3 ions are bonded to the Zr ion.

In the case where the $SmO_{1.5}$ content increases beyond 50 mol%, a certain proportion of the Zr ions on the 16*c* sites must now be replaced with Sm ions (10 mol%, for example, in the case of the end-member 55 mol% $SmO_{1.5}$ pyrochlore) while simultaneously a coupled proportion of the oxygen atoms (nominally 0.1 per formula unit for the 55 mol% $SmO_{1.5}$ pyrochlore) must be extracted (see Table 1). Sm's on the 16*c* sites will, of necessity, be heavily overbonded (AV $\sim$ 5.8 instead of the ideal 3 without a change in x or lattice parameter). If we assume the O1 sites stay fully occupied then the only way to improve the apparent valence (V_i) of these Sm ions is to increase x or to expand the cell parameter or both. Increasing x also increases the O1 contribution to the valence of the Sm ion on the 16*d* site so that it becomes possible for an O2 site surrounding such a Sm ion to be occasionally vacant in agreement with the requirements of charge balance. On the other hand, increasing x also reduces the contribution of the O1 ions to the valence of the majority Zr ions on the 16*c* site. This decrease in ideal valence cannot be compensated for so that the resultant observed x of 0.348 for the 55 mol% $SmO_{1.5}$ specimen is presumably the best compromise that can be reached. The above conclusions are about as much as can be inferred from the WACBED-determined average structures. Further insight requires the observation and modeling of diffuse intensity caused by local short ordering but is beyond the scope of the current contribution.

ACKNOWLEDGMENTS

One of the authors (YT) is grateful for the award of an Australian Research Council Postdoctoral Fellowship.

REFERENCES

1. M. A. Subramanian, G. Aravamudan, and G. V. Subba Rao, *Prog. Solid State Chem.* **15,** 55 (1983).
2. M. A. Subramanian and A. W. Sleight, *in* "Handbook on the Physics and Chemistry of Rare Earths" (K. A. Gschneidner, Jr. and L. Eyring, Eds.), Vol. 16, Chap. 107, p. 225, 1993.
3. M. Perez y Jorba, *Ann. Chim.* **7,** 511 (1962).

4. M. R. Collongues, M. F. Queyroux, M. Perez, Y. Jorba, and M. J-C. Gilles, *Bull. Soc. Chim. France* **4,** 1141 (1965).
5. A. Rouanet, *Rev. Int. Hautes Temper. Refract.* **8,** 161 (1971).
6. D. Michel, M. Perez y Jorba, and R. Collongues, *Mater. Res. Bull.* **9,** 1457 (1974).
7. D. Michel, M. Perez y Jorba, and R. Collongues, *J. Raman. Spectr.* **5,** 163 (1976).
8. D. J. M. Bevan and E. Summerville, *in* "Handbook on the Physics and Chemistry of Rare Earths," (K. A. Gschneidner, Jr. and L. Eyring, Eds.), Vol. 3, p. 401, North-Holland, Amsterdam, 1979.
9. T. van Dijk, K. J. de Vries, and A. J. Burggraaf, *Phys. Stat. Sol.* **58,** 115 (1980).
10. M. P. van Dijk, K. J. de Vries, and A. J. Burggraaf, *Solid State Ionics* **9 & 10,** 913 (1983).
11. M. P. van Dijk, A. J. Burggraaf, A. N. Cormack, and C. R. A. Catlow, *Solid State Ionics* **17,** 159 (1985).
12. Y. Tabira and R. L. Withers, *Phil. Mag. A* **79**(6), 1335 (1999).
13. Y. Tabira and R. L. Withers, *Phys. Chem. Min.*, in press.
14. H. J. Deiseroth and Hk. Müller-Buschbaum, *Z. Anorg. Chem.* **375,** 152 (1970).
15. D. M. Bird and Q. A. King, *Acta Cryst. A* **46,** 202 (1990).
16. D. Altermatt and I. D. Brown, *Acta Cryst. B* **41,** 240 (1985).
17. N. E. Brese and M. O'Keeffe, *Acta Cryst. B* **47,** 192 (1991).
18. I. D. Brown, *Acta Cryst. B* **33,** 1305 (1977).